scientific reports

Check for updates

OPEN

A Schrödinger and differential evolution framework for PID based liquid level control

Davut Izci[1], Serdar Ekinci[2], İrfan Ökten[2], Vedat Tümen[2], Mostafa Rashdan[3] & Mohammad Salman[3]✉

In this study, a hybrid Schrödinger optimizer with differential evolution (h-SRADE) is proposed for optimal tuning of proportional–integral–derivative (PID) controllers applied to a three-tanks liquid level control system. The original Schrödinger optimizer (SRA), inspired by wave–particle duality and quantum mechanics principles, provides a balanced exploration–exploitation mechanism; however, its convergence sensitivity in the later optimization stages motivates further enhancement. To address this limitation, differential evolution mutation and crossover operators are embedded into the SRA framework, forming the proposed h-SRADE algorithm with improved refinement capability and convergence stability. The control problem is formulated using a linearized third-order model of the three-tanks liquid level system derived from mass balance principles. PID controller parameters are optimized by minimizing a composite fitness function that simultaneously accounts for percent overshoot, steady-state error, settling time, and rise time. The optimization process is conducted within predefined practical bounds to ensure controller feasibility and robust closed-loop operation. Extensive simulation studies are carried out to evaluate the performance of the proposed method. Statistical analysis, supported by a non-parametric Wilcoxon signed-rank test, confirms the statistical significance and robustness of h-SRADE over the conventional SRA. Time-domain and frequency-domain analyses demonstrate that the h-SRADE-based PID controller achieves faster settling, reduced overshoot, lower steady-state error, and satisfactory robustness margins. Furthermore, comparative studies with several state-of-the-art optimization-based PID tuning approaches reported in the literature reveal that the proposed method provides superior dynamic performance and overall control quality. The obtained results indicate that the hybridization of the Schrödinger optimizer with differential evolution effectively enhances convergence behavior and control performance. Consequently, the proposed h-SRADE framework offers a reliable and efficient simulation-based solution for PID controller tuning in liquid level systems, providing a strong foundation for future extension toward nonlinear plant models, varying operating points, and other complex engineering control applications.

Keywords Liquid level control, Schrödinger optimizer, Proportional–integral–derivative controller, Differential evolution, Hybridization

Liquid level control constitutes a fundamental problem in process industries such as chemical processing, power generation, water treatment, and petrochemical systems, where accurate regulation is essential to guarantee operational safety, product quality, and overall system efficiency[1]. In many industrial installations, improper liquid level regulation may result in safety hazards, equipment damage, or degradation of process performance. Consequently, liquid level systems have long served as benchmark processes for the development and evaluation of advanced control strategies[2]. Among these benchmarks, multi-tank liquid level systems have received particular attention due to their nonlinear behavior, inter-tank coupling, large inertia, and sensitivity to parameter variations and external disturbances[3–6].

In particular, the three-tank liquid level system has emerged as a representative and widely accepted test platform for validating control and optimization methodologies[7–12]. Owing to its higher-order dynamics and

[1]Department of Electrical and Electronic Engineering, Bursa Uludag University, 16059 Bursa, Turkey. [2]Department of Computer Engineering, Bitlis Eren University, 13100 Bitlis, Turkey. [3]College of Engineering and Technology, American University of the Middle East, 54200 Egaila, Kuwait. ✉email: mohammad.salman@aum.edu.kw

inherent nonlinearities, the three-tank system accurately reflects the challenges encountered in real industrial processes. As reported in several studies, the interacting nature of such systems makes controller design nontrivial, especially when strict transient and steady-state performance requirements must be satisfied simultaneously[13–15]. For this reason, the three-tank liquid level process has been extensively employed to benchmark both classical and intelligent control approaches.

Proportional–integral–derivative (PID) controllers remain the most widely adopted control structures in industrial practice, accounting for the majority of deployed feedback controllers due to their simple structure, intuitive tuning, and robustness against moderate uncertainties[16–20]. Despite these advantages, conventional PID controllers often struggle to deliver satisfactory performance when applied to nonlinear and higher-order systems such as multi-tank liquid level processes. It has been consistently reported that classical tuning rules may lead to excessive overshoot, prolonged settling times, or poor disturbance rejection, particularly when the operating point varies or system parameters change[21]. As a result, controller performance becomes highly dependent on the tuning strategy employed.

To overcome these limitations, the PID tuning problem has increasingly been formulated as an optimization task, thereby motivating the application of metaheuristic algorithms[22]. In recent years, numerous population-based optimization techniques have been successfully applied to PID controller design for liquid level systems. These include genetic algorithms, particle swarm optimization, sine–cosine algorithm, grey wolf optimization, salp swarm algorithm, prairie dog optimization, and African vulture optimization, among others[14,15,23,24]. Such methods offer derivative-free search mechanisms capable of addressing nonlinearity, multimodality, and complex constraint landscapes, which are commonly encountered in control parameter optimization.

Hybrid optimization strategies have also gained increasing attention. By combining complementary exploration and exploitation mechanisms, hybrid algorithms have demonstrated improved convergence speed, enhanced solution quality, and superior robustness[25–27]. Notable examples include hybrid differential evolution and particle swarm optimization with an aging leader and challengers[28], hybrid arithmetic and Harris hawks optimization[29], and enhanced artificial satellite search algorithm with memory and evolutionary operator[30]. Although these approaches have achieved promising results, many studies report that premature convergence or insufficient refinement capability may still occur during later stages of optimization, particularly for complex control problems with tightly coupled performance objectives.

The Schrödinger optimization algorithm (SRA)[31] is a relatively recent metaheuristic inspired by wave–particle duality and fundamental concepts of quantum mechanics. By alternately employing probabilistic wave-like exploration and deterministic particle-like exploitation behaviors, SRA provides a flexible mechanism for balancing global search and local refinement. This dual-mode structure has been shown to enhance exploration efficiency in complex search spaces. However, as observed in challenging optimization scenarios, the refinement capability of SRA may weaken during the final stages of the search process, which can limit solution accuracy and convergence stability.

Differential evolution (DE), on the other hand, is a well-established population-based optimization algorithm recognized for its strong local search capability, simplicity, and robustness in continuous optimization problems[32]. The mutation and crossover operators of DE introduce effective corrective movements that enhance exploitation while preserving population diversity. DE has been successfully integrated into various hybrid frameworks to improve convergence reliability and fine-tuning precision[33–35]. Consequently, combining DE with SRA represents a promising strategy to strengthen local refinement without compromising global exploration.

Motivated by these observations, this study proposes a hybrid Schrödinger optimizer with differential evolution, referred to as h-SRADE, for optimal PID controller tuning. In the proposed framework, DE mutation and crossover operators are embedded within the SRA search process to facilitate smoother transitions from exploration to exploitation and to mitigate stagnation near local optima. The effectiveness of the proposed approach is investigated through its application to a three-tank liquid level control system modeled using a linearized third-order dynamic representation derived from mass balance principles.

The PID controller parameters are optimized using a composite fitness function that simultaneously accounts for transient and steady-state performance indices, including percent overshoot, steady-state error, settling time, and rise time. Comprehensive simulation studies are conducted to evaluate convergence behavior, statistical robustness, time-domain and frequency-domain performance, and comparative effectiveness against state-of-the-art optimization-based PID tuning approaches reported in the literature, including hybrid differential evolution and particle swarm optimization with an aging leader and challengers[28], hybrid arithmetic and Harris hawks optimization[29], mountain gazelle optimization[23] and enhanced artificial satellite search algorithm with memory and evolutionary operator[30].

To verify the effectiveness of the proposed h-SRADE framework, an extensive set of simulation-based analyses is performed throughout the study. The convergence behavior and robustness of the optimization process are first examined through repeated independent runs, supported by statistical performance indicators and a non-parametric Wilcoxon signed-rank test. The evolution of the fitness function and PID controller parameters is then analyzed to assess convergence stability and parameter adaptation characteristics. Furthermore, the closed-loop system performance is evaluated in both the time and frequency domains, where key dynamic indices such as settling time, percent overshoot, steady-state error, gain margin, and phase margin are examined in detail. Comparative studies are also conducted against the original Schrödinger optimizer and several state-of-the-art hybrid optimization-based PID tuning approaches reported in the literature. The obtained results consistently demonstrate that the proposed h-SRADE-based PID controller achieves faster settling, reduced overshoot, improved steady-state accuracy, and competitive robustness margins, while yielding the lowest overall fitness function value among all compared methods. These analyses collectively confirm the effectiveness, robustness, and superior control quality of the proposed approach.

In light of the above discussion, the main contributions of this study can be summarized as follows: (i) the development of a novel hybrid optimization framework that integrates Schrödinger-based search dynamics with differential evolution refinement mechanisms; (ii) the formulation of a robust PID tuning strategy for a three-tank liquid level system using a multi-objective, performance-oriented fitness function; and (iii) a thorough statistical, dynamic, and comparative evaluation demonstrating the superiority of the proposed method over existing approaches.

The remainder of the paper is organized as follows. Section "Schrödinger optimizer" presents the fundamentals of the Schrödinger optimization algorithm. Section "Hybrid Schrödinger optimizer with differential evolution (h-SRADE)" introduces the proposed h-SRADE framework and its hybridization mechanism. Section "Case study" describes the modeling of the three-tank liquid level system and the PID-based control structure. Section "Proposed control approach" details the proposed control and optimization approach. Simulation results and performance analyses are discussed in Section "Simulation results". Finally, conclusions and potential directions for future research are provided in Section "Conclusion".

Schrödinger optimizer

The Schrödinger optimization algorithm (SRA) is a meta-heuristic optimization algorithm developed inspired by wave-particle duality, one of the fundamental principles of quantum mechanics, and the Schrödinger equation. Wave-particle duality is a quantum mechanical method with the double-slit experiment that exhibits both wave and particle properties of fundamental particles such as electrons and photons[31]. When unobserved, particles exhibit wave-like behavior, creating interference patterns, while when observed, these wave properties disappear and the behavior reverts to particle properties. SRA translates this physical phenomenon into an optimization context, offering an innovative approach that considers the behavior of search agents. In the algorithm, search agents sometimes behave in a wave-like manner, i.e., with a probabilistic and uncertain update mechanism, while in other cases they update their positions in a particle-like manner, i.e., with a deterministic method. Instead of precise and singular actions, search agents perform a search process involving multiple probabilities, thus reducing the risk of early lock-in to local best solutions, especially on multi-peak and complex fitness surfaces. In contrast, in the particle-like behavior regime, the algorithm makes deterministic updates based on classical mechanics principles inspired by Newton's second law. This approach improves the solution, increasing its exploitability. SRA's most distinctive feature is its ability to combine these two update structures under a single algorithmic framework and adaptively switch between wave and particle behaviors depending on the context of the search process. SRA stands out as a unique and innovative approach in the literature due to both its strong theoretical foundation and the integrated use of quantum and classical mechanics principles. Additionally, SRA provides a more flexible and effective search in multimodal optimization scenarios. In this study, SRA was used to optimize controller parameters in a liquid level control problem. The aim is to explore the solution space with wave-like probabilistic updates in the initial iterations and then improve control performance with particle-like deterministic updates in subsequent iterations, achieving a balanced optimum solution between reference level tracking, over-oscillation, and control effort criteria. In the SRA optimization algorithm, as the iterations progress, a large portion of the population gradually transitions from exploration to exploitation. The SRA consists of the following processes: Initialization, Wave function selection, Exploration update, Rank/probability sequence, Exploitation update, Random restart, and Transition from exploration to exploitation. The Initialization phase directly affects the algorithm's exploration ability in early iterations, thus forming the basis of solution quality and convergence behavior. In this phase, as seen in Eq. (1), the initial position of each search agent in the population is randomly selected within variable lower/upper bounds to cover a large portion of the search space by providing initial diversity.

$$x_i = lb + rand \cdot (ub - lb) \tag{1}$$

In Eq. (1), $rand \in (0,1)$ is the random number, lb and ub are the lower/upper limit vectors. Since it is difficult to directly use the solution of the Schrödinger equation in the exploration phase, a simple representation for the wave function is chosen as shown in Eq. (2).

$$\psi(x_i, t) = \sin(x_i) \tag{2}$$

Equation (2) produces a particle-like periodic wave behavior for infinite potential states, while ψ modulates the step magnitude and direction in a "probabilistic/wave-like" manner during the exploration update. The "wave-like" update of the SRA during the exploration update phase is provided in two variants.

$$x_{i+1} = x_{best} + \left[rand \cdot {}_{\varkappa c} \cdot \frac{h \cdot (\psi(x_{best}, t) - \psi(x_{worst}, t)) + p[i] \cdot (\psi(x_{rand1}, t) - \psi(x_i, t) + \psi(x_{rand2}, t))}{\psi(x_i, t)} \right] \tag{3}$$

$$x_{i+1} = x_i + \left[rand \cdot {}_{\varkappa c} \cdot \frac{h \cdot (\psi(x_{best}, t) - \psi(x_{worst}, t)) + p[i] \cdot (\psi(x_{rand1}, t) - \psi(x_i, t) + \psi(x_{rand2}, t))}{\psi(x_i, t)} \right] \tag{4}$$

Equations (3) and (4) show that $\psi(x_{best}, t)$ is considered the best position and $\psi(x_{best}, t)$ the worst position; $\psi(x_{rand1}, t)$ and $\psi(x_{rand2}, t)$ are the wave function values of two randomly selected positions from the population. ${}_{\varkappa c}$ represents a linearly decreasing coefficient from 1 to 0. Here, the new position is determined as x_{best}; this allows for "wide searching around good regions" without leaving the exploration to uncontrolled expansion. The new position is updated via x_i; that is, the agent can make wave-like jumps in its own region. $rand \cdot {}_{\varkappa c}$ reduces the step (cooling over time) as the iteration progresses. $h \cdot (\psi(x_{best}) - \psi(x_{worst}))$ repositions

the population more distinctly as the difference between the best and worst wave values increases. Here, h can be considered a scale inspired by the physical Planck constant. $p[i] \cdot (\psi(x_{rand1}) - \psi(x_i, t) + \psi(x_{rand2}))$ generates a variation that allows jumping to new regions on multimode surfaces in the wave space via two random agents and the current agent. The value of $\psi(x_i)$ in the denominator normalizes with respect to the wave amplitude of the current position; it can produce behaviors such as "large jumps if the amplitude of the wave function is small". The probability sequence, which is the weight to be used in the selection between exploration and exploitation updates, is given in Eq. (5).

$$p[i] = \left(\frac{N-i}{N}\right)^2, i = 0, 1, \ldots N-1 \tag{5}$$

Here, N is the population size, and i is considered as the index in the ranked population. As i increases, $p[i]$ decreases rapidly; that is, $p[i]$ is larger for good solutions and smaller for bad solutions. $p[i]$ ensures that the wave update and transition decision become adaptive with the "agent quality/rank". Equation (6) has been developed for the exploitation update.

$$x_{i+1} = k \cdot rand + 2 \cdot x_i - x_{i-1} \tag{6}$$

In Eq. (6), k is the scale factor (in most cases $k = 1$ is chosen). $2 \cdot x_i - x_{i-1}$, due to the second difference structure, gives the agent inertial/momentum-like behavior, giving it a tendency to maintain the previous step direction. The k scale factor adds stochasticity to prevent premature convergence. To avoid falling into a regional solution, Eq. (7) needs to be included.

$$x_{i+1} = x_{best} - rand \cdot (x_{rand1} - x_{rand2}) \tag{7}$$

In this equation, x_{best} represents the best position the particle has ever reached, and x_{rand1} and x_{rand2} represent two different positions randomly selected from the population. The Schrödinger equation describes the evolution of a system's wave function over time, treating the particle's position in a probabilistic rather than a precise value. In contrast, in classical mechanics, the particle's position is determined deterministically by Newton's equations of motion. When the amplitude of the wave packet is sufficiently small, the Schrödinger equation can be reduced to Newton's equation of motion. This physical interpretation forms the basis for the transition in SRA from wave-like probabilistic updates in the exploration phase to particle-like deterministic updates in the exploitation phase, enabling the algorithm to effectively balance global search with local refinement. However, despite the balanced operation of exploration and exploitation mechanisms, an additional random update mechanism is defined in Eq. (8) to prevent the algorithm from getting stuck in local optima and to maintain population diversity.

$$x_{i+1} = rand \cdot (ub - lb) + lb if rand < 0.03 \tag{8}$$

Here, $rand$ represents a uniform random number generated in the range $(0,1)$. This completely random reboot step, implemented with a 3% probability, allows the algorithm to avoid local optima while contributing to the preservation of diversity within the population. The low probability value ensures that this mechanism rarely kicks in, preventing it from negatively impacting the stability and convergence behavior of the main optimization process. The transition between the exploration and exploitation phases in SRA is based on a finite sequence $p[i]$ given in Eq. (5) and is controlled by a threshold function defined depending on the number of iterations. This threshold function, given in Eq. (9), increases rapidly from values close to zero to one as the iteration progresses.

$$TF(t) = \left(\frac{t}{t_{max}}\right)^3 \tag{9}$$

When Eq. (9) is examined, $TF(t)$ increases rapidly from 0 to 1 as the iteration increases. In Eq. (5):

- If $p[i] \geq TF(t)$, then the wave-like update in Eqs. (3) and (4) is performed,
- If $p[i] < TF(t)$, then the particle-like update in Eq. (6) and (7) is performed,

Initially, since $TF(t)$ is small, $p[i] \geq TF(t)$ holds for many agents, and the population is predominantly exploration oriented. As $TF(t)$ grows over time, the condition $p[i] \geq TF(t)$ becomes more difficult to satisfy, and the population becomes increasingly exploitation-oriented.

Hybrid Schrödinger optimizer with differential evolution (h-SRADE)

Differential evolution algorithm

Differential evolution (DE) is known as a population-based stochastic optimization method and has become increasingly popular due to its good performance in continuous and nonlinear search domains[36]. Instead of relying on gradient information, DE improves solutions through simple vector operations; therefore, it can solve non-differentiable and multimodal problems more effectively than many classical techniques. The basic working idea is quite simple: differences between randomly selected individuals are scaled and transferred to other candidates, generating new solution vectors. This mechanism naturally encourages both the exploration of unexplored regions and the utilization of promising areas of the search domain. Optimization begins with a population of N candidate solutions, each as a real-valued vector of dimension m. These vectors are distributed within predefined upper and lower bounds for the decision variables. These are constructed as follows.

$$X_i = lb_j + r \cdot (ub_j - lb_j), i = 1, 2, \ldots, N, j = 1, 2, \ldots, m \tag{10}$$

In this context, lb_j and ub_j denote the lower and upper bounds of the j-th variable, and r is a random number.

Once the process begins, DE improves the population through mutation and crossover operations. In the mutation phase, a mutant vector V_i is generated for each target vector X_i using three distinct individuals X_{rand1}, X_{rand2}, and X_{rand3} randomly selected from the population:

$$V_i = X_{rand1} + F \cdot (X_{rand2} - X_{rand3}) \tag{11}$$

where F is the mutation scaling factor controlling the amplification of the differential variation.

Subsequently, a crossover operation is applied to produce a trial vector U_i by combining components of the mutant vector V_i and the target vector X_i:

$$U_{i,j} = \begin{cases} V_{i,j}, if r_j \leq CR or j = j_{rand}, \\ X_{i,j}, otherwise \end{cases} \tag{12}$$

where CR is the crossover probability, $r_j \in [0,1]$ is a random number, and j_{rand} is a randomly selected index that guarantees at least one component from the mutant vector is inherited by the trial vector.

In the selection phase, the fitness of the trial vector U_i is compared with that of the target vector X_i. The individual yielding the better objective function value is retained for the next generation:

$$X_i = \begin{cases} U_i, if f(U_i) < f(X_i) \\ X_i, otherwise \end{cases} \tag{13}$$

This mechanism systematically guides the population toward optimal solution regions by ensuring that only solutions with higher efficiency are preserved in subsequent iterations.

Hybrid SRA with DE

The proposed h-SRADE integrates the DE mutation and crossover operators as a systematic refinement layer within the SRA iterative framework. The motivation for this hybridization stems from the observation that, although SRA provides effective global exploration through its wave-like probabilistic updates, the population's refinement capability tends to weaken in the later iterations when agents cluster around promising regions. By embedding DE operators at the conclusion of each SRA update cycle, the algorithm is endowed with a corrective search mechanism that enhances local exploitation without disrupting the global search dynamics established by SRA.

The integration is structured as follows. At each iteration *t*, every agent first undergoes the standard SRA positional update (either the wave-like update defined by Eqs. (3) and (4) or the particle-like update defined by Eqs. (6) and (7)) according to the transition function $TF(t)$ given in Eq. (9) and the rank-based probability $p[i]$ from Eq. (5). Additionally, the random restart mechanism of Eq. (8) is applied with its prescribed probability. After all agents have completed their SRA-based updates and the population has been evaluated, the DE refinement step is applied universally to all agents in the population without exception.

For each agent i, a mutant vector V_i is constructed according to the DE mutation scheme of Eq. (11), where three distinct agents X_{rand1}, X_{rand2}, and X_{rand3} are selected uniformly at random from the current population, excluding agent i itself. The mutation scaling factor is set to $F = 0.5$, a value well established in the DE literature for continuous optimization and adopted in prior hybrid frameworks involving DE refinement for control parameter tuning[37–39]. A binomial crossover operation is subsequently applied to produce a trial vector U_i by combining components of V_i and the current agent position X_i according to Eq. (12), with the crossover probability set to $CR = 0.9$. This relatively high crossover rate promotes diversity in the trial vector while ensuring that the mutant vector's directional information is effectively inherited. The index j_{rand} in Eq. (12) guarantees that at least one component of V_i is present in U_i, preventing a trivial crossover outcome.

Following the generation of U_i, a greedy selection is performed in accordance with Eq. (13): if the fitness of the trial vector U_i is lower than that of the current position X_i, the trial vector replaces X_i in the population; otherwise, the original position is retained. This selection criterion ensures that the DE refinement step is strictly non-deteriorating, so the population quality is preserved or improved at every iteration. The trial vector generation and selection are applied independently to every agent before the population proceeds to the next iteration, thereby maintaining population integrity throughout the optimization process.

The DE parameters $F = 0.5$ and $CR = 0.9$ were selected based on established guidelines for DE in continuous optimization[32] and validated empirically across preliminary runs on the present control problem. These values are consistent with those employed in related hybrid DE frameworks reported in the literature[38,39] and were found to provide a reliable balance between perturbation magnitude and genetic material inheritance across the population.

Beyond its empirical effectiveness, the hybridization of SRA with DE is also motivated by a structural complementarity between the two mechanisms. The wave-like exploration update of SRA, governed by Eqs. (3) and (4), generates new agent positions through amplitude-modulated perturbations derived from the sinusoidal wave function, and these positions are adopted unconditionally, without reference to whether they improve the agent's fitness. While this property is essential for maintaining broad exploration in the early search stages, it also means that, as the population transitions toward the particle-like exploitation regime governed by $TF(t)$, favourable positions identified through SRA's update rules may be displaced by subsequent unconditional moves rather than preserved and refined. The DE operators embedded at the end of each iteration address this

gap directly: the mutation and crossover steps (Eqs. 11–12) generate trial vectors informed by the differential structure of the current population, and the greedy selection criterion of Eq. (13) ensures that only non-deteriorating trial vectors are retained. In this respect, the role of DE within h-SRADE is not merely to add an additional search operator, but to act as a fitness-gated stabilization layer for an algorithm whose native update equations are themselves fitness-agnostic at the point of application. This structural complementarity, in addition to the empirical performance gains demonstrated in Section "Simulation results", provides a principled justification for the proposed hybridization.

The overall effect of this integration is a smooth and progressive transition from SRA's broad exploration to increasingly focused exploitation as the iteration count advances. In the early iterations, $TF(t)$ is small, so the majority of agents undergo wave-like updates and explore the search space broadly; the DE refinement step provides only marginal corrections at this stage, as agents are still dispersed. As $TF(t)$ grows, more agents transition to particle-like updates and begin converging toward promising regions, at which point the DE operators become increasingly active in refining individual positions and correcting stagnation. This layered mechanism ensures that the h-SRADE framework is neither prematurely exploitative nor excessively stochastic near convergence. Figure 1 provides a visual representation of this workflow, illustrating the sequential interaction between the SRA update phase and the DE refinement phase within each iteration cycle. The flowchart, together with the algorithmic description above and the mathematical formulations in Sections "Schrödinger optimizer" and "Differential evolution algorithm", constitutes a complete and reproducible specification of the h-SRADE procedure.

Case study

Modeling of three-tanks liquid level system

The three-tanks liquid level system considered in this study is a well-known benchmark nonlinear process widely used to evaluate advanced control and optimization strategies[28]. The schematic representation of the system is illustrated in Fig. 2. The overall structure consists of three interconnected process tanks, denoted as Tanks B, C, and D, which are supplied by a main reservoir tank (Tank E). The liquid is circulated through the system by means of electrically actuated valves and pumps, enabling regulation of the liquid level within the tanks.

In order to control the liquid level, the error between the desired reference level and the measured liquid height is first computed. This error signal is then processed by a controller, which generates a control action to adjust the opening range of the electric valve. The valve opening varies continuously between 0 and 100%, thereby modifying the inlet flow rate and regulating the liquid level dynamics of the system.

A simplified dynamic model of an individual tank is obtained using the mass balance principle. Considering Tank D as a representative unit, the conservation of mass can be expressed as the difference between the inlet and outlet flow rates, yielding

$$q_2 - q_1 = A\frac{dh}{dt} \tag{14}$$

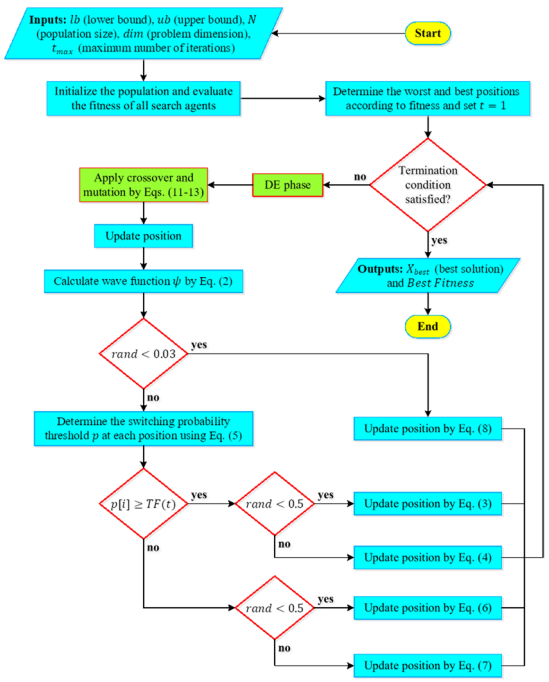


Fig. 1. Flowchart of h-SRADE

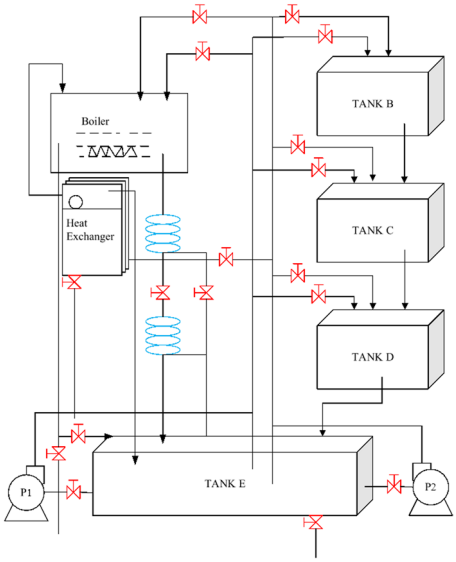


Fig. 2. Schematic representation of the three-tank liquid level system

where q_1 and q_2 denote the inlet and outlet flow rates, respectively, A represents the cross-sectional area of the tank, and h is the liquid level.

The inlet flow rate is assumed to be proportional to the valve opening range and is given by:

$$q_1 = k_1 v_o \tag{15}$$

where v_o denotes the valve opening signal and k_1 is the corresponding flow proportional coefficient. The outlet flow rate depends nonlinearly on the liquid height and is modeled as:

$$q_2 = k_2 \sqrt{h} \tag{16}$$

with k_2 being the flow proportional coefficient associated with the outlet orifice. Equations (14)–(16) indicate that the liquid level dynamics exhibit inherent nonlinearity due to the square-root dependence of the outlet flow rate on the liquid height. To facilitate controller design and performance analysis, the system is linearized around an operating equilibrium point (VO_0, h_0). Near this operating point, the nonlinear outlet flow can be approximated as:

$$\frac{q_2}{h} \approx \frac{k_2}{\sqrt{h_0}} = k_3 \tag{17}$$

where k_3 represents an equivalent linear flow coefficient. Applying the Laplace transform to the linearized equations results in a first-order transfer function between the valve opening signal and the liquid level for a single tank, expressed as:

$$\frac{H(s)}{VO(s)} = \frac{k}{Ts+1} \tag{18}$$

where $k = \frac{k_1}{k_3}$ and $T = \frac{A}{k_3}$. For the parameter values $k_1 = 2$, $k_3 = 5$, and $A = 20$, the resulting single-tank dynamics are obtained. Considering the cascaded interconnection of the three tanks, the overall transfer function of the three-tanks liquid level system can be expressed as given in Eq. (19).

$$G(s) = \frac{1}{(4s+0.2)^3} = \frac{1}{64s^3 + 9.6s^2 + 0.48s + 0.008} \tag{19}$$

This third-order transfer function accurately represents the linearized dynamics of the complete three-tanks liquid level system and serves as the plant model for the controller design and optimization procedures discussed in the subsequent sections.

Liquid level system with PID controller

In this study, a PID controller is employed to regulate the liquid level of the three-tanks system modeled in the previous subsection. Owing to its simple structure, robustness, and widespread industrial acceptance, the PID controller remains one of the most commonly used control strategies for liquid level processes and other industrial applications. The control action generated by the PID controller is based on the error signal, defined as

the difference between the reference liquid level and the measured tank level. In the Laplace domain, the transfer function of the PID controller is expressed as[40]:

$$C(s) = K_p + \frac{K_i}{s} + K_d s \tag{20}$$

where K_p, K_i, and K_d denote the proportional, integral, and derivative gains, respectively. The proportional term provides an immediate response to the current error, the integral term eliminates steady-state error by accumulating past error values, and the derivative term improves transient performance by anticipating future error trends.

The closed-loop structure of the liquid level control system incorporating the PID controller is illustrated in Fig. 3. As shown in the block diagram, the reference signal $r(t)$ is compared with the measured output $y(t)$ to generate the error signal $e(t)$. This error is processed by the PID controller to produce the control input $u(t)$, which actuates the industrial process represented by the three-tanks liquid level plant. The system output is then fed back to ensure continuous regulation of the liquid level.

By combining the PID controller with the linearized plant model derived in the previous section, a complete feedback control framework is established. This structure enables systematic evaluation of both transient and steady-state performance characteristics and provides a suitable basis for the controller parameter optimization procedures introduced in the subsequent sections. The PID controller formulation and its integration within the liquid level control loop are consistent with standard control practice and recent literature on liquid level regulation problems.

Proposed control approach

In this study, the tuning of the PID controller parameters is formulated as an optimization problem and addressed using the proposed h-SRADE. The objective of the optimization process is to obtain PID parameters that provide a balanced trade-off between transient response quality and steady-state accuracy for the three-tanks liquid level system. To quantitatively evaluate control performance, a composite fitness function (FF) is adopted, which incorporates multiple time-domain performance indices. The fitness function is defined as[41]:

$$FF = \left(1 - e^{-\varphi}\right)\left(\frac{m_{os} + e_{ss}}{100}\right) + e^{-\varphi}\left(t_{set} - t_{rise}\right) \tag{21}$$

where φ is a weighting factor selected as $\varphi = 1$. In this formulation, m_{os} denotes the percentage overshoot, e_{ss} represents the percentage steady-state error evaluated at the end of the simulation time ($t_{sim} = 250$ s), t_{set} is the settling time calculated within a ± 2% tolerance band, and t_{rise} is the rise time measured between 10 and 90% of the final value. The adopted fitness function enables simultaneous consideration of both transient and steady-state characteristics. The first term penalizes excessive overshoot and steady-state error, while the second term emphasizes fast system response by accounting for settling and rise times. Through the exponential weighting factor, the contribution of these two components is smoothly balanced, preventing dominance of a single performance index and promoting overall control quality. The weighting factor φ acts solely as a trade-off parameter between these two components, since the coefficients are complementary and vary monotonically with φ. Larger values shift the emphasis toward the suppression of overshoot and steady-state error, whereas smaller values favour a faster response by increasing the influence of the settling and rise time term. The value $\varphi = 1$ adopted here was designated on the basis of extensive trial-and-error evaluations carried out during the development of the present study. In these preliminary investigations, the controller gains were re-optimized for a range of candidate weightings and the resulting closed-loop responses were assessed with respect to overshoot, steady-state accuracy, settling and rise times. Lower values of φ were observed to yield faster but less adequately damped responses, whereas higher values suppressed overshoot at the cost of a noticeably sluggish approach to the reference level. The selected value was found to provide the most favorable overall compromise for the three-tank liquid level process considered here, and no alternative weighting examined produced a demonstrably better outcome/

During the optimization process, the h-SRADE algorithm iteratively updates the PID controller gains (K_p , K_i, and K_d) to minimize the fitness function defined in Eq. (21). The search is conducted within predefined parameter bounds to ensure physically meaningful and practically implementable controller gains. The adopted ranges are given as $0.01 \leq K_p \leq 0.1$, $0.0001 \leq K_i \leq 0.001$, and $0.1 \leq K_d \leq 0.5$. These limits are selected based on system dynamics and prior studies to avoid controller saturation, instability, or excessive control effort.

It is also worth noting that the valve opening signal, which constitutes the physical actuation variable of the three-tank system, is inherently restricted to the range of 0% to 100%, as described in Section "Modeling

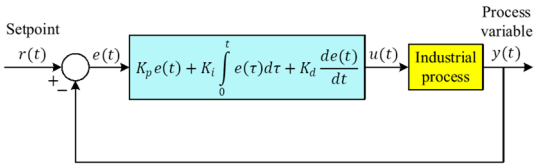


Fig. 3. Liquid level system with PID controller

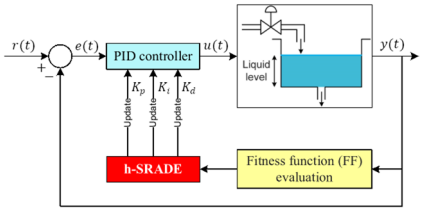


Fig. 4. Representation of liquid level system control via h-SRADE-optimized PID control method

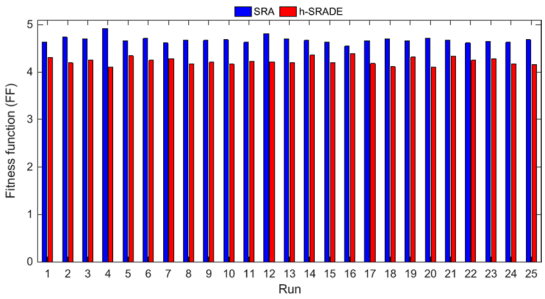


Fig. 5. Fitness function evaluation across 25 runs for SRA and h-SRADE

of three-tanks liquid level system". The PID gain bounds adopted in this study were deliberately selected to be conservative with respect to this physical limitation, such that the control signals generated for the step-response scenarios considered in Section "Simulation results" remain within the admissible actuation range, and no saturation of the valve was encountered during the reported simulations. The PID controller employed in this study is an ideal, unfiltered structure, as reflected in Eq. (20), and does not incorporate an explicit anti-windup mechanism. Under the operating conditions examined here, this does not compromise the validity of the reported results, since the control effort remains within the linear operating region of the actuator throughout the simulation horizon. However, it is acknowledged that, should the controller be applied to larger reference changes, significant load disturbances, or the full nonlinear plant dynamics, the control signal could approach or exceed the physical valve limits, in which case integrator windup may occur and degrade transient performance. In such cases, the inclusion of an anti-windup strategy, such as integrator clamping or a back-calculation scheme, would be necessary to prevent excessive overshoot and prolonged recovery following saturation events. This consideration is identified as a relevant extension of the present framework and is discussed further in Section "Conclusion".

The overall structure of the proposed control approach is illustrated in Fig. 4. As shown, the reference signal is compared with the measured liquid level to generate the error signal, which is processed by the PID controller. The controller gains are continuously adjusted by the h-SRADE algorithm based on the evaluated fitness function. This closed-loop optimization framework allows direct assessment of control performance through time-domain simulations and ensures that the resulting PID parameters are optimally tuned with respect to the defined performance criteria. The proposed control strategy provides a systematic and flexible framework for PID tuning in nonlinear liquid level systems and forms the basis for the simulation studies and comparative analyses presented in the subsequent sections.

Simulation results

Statistical analysis and non-parametric test

To evaluate the robustness and reliability of the proposed h-SRADE, a comprehensive statistical analysis was conducted and compared with the original SRA. For both algorithms, 25 independent runs were performed using a population size of 30 and a maximum iteration number of 100. In each run, the fitness function defined in Eq. (21) was minimized by tuning the PID controller parameters within the prescribed bounds. The distribution of fitness function values obtained across the 25 runs for both algorithms is illustrated in Fig. 5. As observed, the h-SRADE consistently yields lower fitness values compared to SRA in almost all runs, indicating superior convergence behavior and enhanced solution quality. The reduced dispersion of results further suggests that the hybrid algorithm exhibits improved robustness against stochastic variations inherent in population-based optimization methods.

The quantitative statistical results are summarized in Table 1, which reports the best, worst, average, and standard deviation (SD) of the fitness function values for both algorithms. The best fitness value achieved by h-SRADE is 4.1068, which is significantly lower than that obtained by SRA (4.5501). Similarly, the average fitness value of h-SRADE (4.2332) is markedly smaller than that of SRA (4.6816), confirming the overall performance improvement introduced by the hybridization strategy. Although the standard deviation of h-SRADE is slightly higher than that of SRA, the difference remains small and does not undermine the observed performance gains.

Algorithm	Best	Worst	Average	SD	*p*-value
SRA	4.5501	4.9228	4.6816	0.0706	1.2290E-05
h-SRADE	4.1068	4.3881	4.2332	0.0791	–

Table 1. Statistical performance of the SRA and h-SRADE and related Wilcoxon's test.

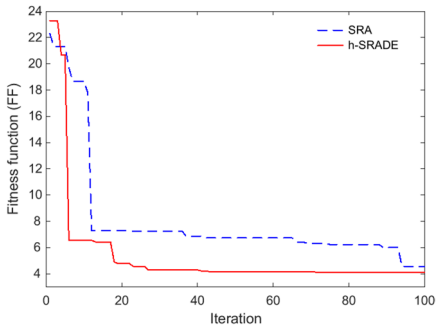


Fig. 6. Convergence of fitness function

To statistically validate the significance of the performance improvement, a non-parametric Wilcoxon signed-rank test was applied. The resulting p-value of 1.2290×10^{-5} indicates a statistically significant difference between the two algorithms at conventional significance levels. This outcome confirms that the observed reduction in the fitness function achieved by h-SRADE is not due to random chance but results from the enhanced search and refinement capabilities provided by the integration of differential evolution operators.

In addition to solution quality, the computational cost of the two algorithms was also recorded across the 25 independent runs. The average elapsed wall-clock time per run was 353.07 s for SRA and 360.69 s for h-SRADE, corresponding to a computational overhead of approximately 2.16% for the proposed hybrid algorithm. This marginal increase in runtime is a direct consequence of the additional DE mutation, crossover, and selection operations performed for every agent at the end of each iteration. Given that this modest overhead is accompanied by a 9.58% reduction in the mean fitness function value and by a complete non-overlap of the fitness distributions of the two algorithms across all runs, the additional computational cost incurred by h-SRADE is considered negligible relative to the consistency and magnitude of the performance improvement achieved. Overall, the statistical analysis demonstrates that the proposed h-SRADE algorithm outperforms the conventional SRA in terms of solution quality, convergence consistency, and statistical significance. These findings justify the adoption of the hybrid optimization framework for PID controller tuning in the three-tanks liquid level control problem and provide a solid foundation for the detailed convergence and dynamic response analyses presented in the subsequent subsections.

Change of fitness function and PID controller parameters

The convergence characteristics of the fitness function for both the conventional SRA and the proposed h-SRADE are illustrated in Fig. 6. As observed, the h-SRADE exhibits a markedly faster reduction in the fitness function during the early iterations, indicating an enhanced exploration capability and an efficient transition toward promising regions of the search space. In contrast, the SRA demonstrates a slower convergence rate and remains at comparatively higher fitness levels throughout the optimization process. As the iteration number increases, the fitness function of h-SRADE stabilizes at a significantly lower value, confirming its superior convergence behavior and improved solution quality.

The evolution of the proportional gain K_p over the optimization iterations is presented in Fig. 7. For the SRA, noticeable oscillations and abrupt variations in K_p are observed, particularly during the initial and final stages of the search, which indicate less stable parameter adaptation. Conversely, the h-SRADE shows a smoother and more gradual adjustment of K_p, converging toward a stable value with minimal fluctuations. This behavior reflects the improved balance between exploration and exploitation achieved through the hybridization with differential evolution operators.

The variation of the integral gain K_i throughout the optimization process is depicted in Fig. 8. Similar to the behavior observed for K_p, the SRA exhibits pronounced fluctuations in K_i, especially in the early iterations, before slowly converging. In contrast, the h-SRADE rapidly guides K_i toward a stable region and maintains consistent parameter updates in subsequent iterations. This stable convergence is particularly important for liquid level control applications, as excessive variations in the integral gain may lead to windup effects and degraded steady-state performance.

The evolution of the derivative gain K_d, shown in Fig. 9, further highlights the advantages of the proposed hybrid approach. The SRA displays irregular changes and delayed convergence of K_d, whereas the h-SRADE achieves a smooth and monotonic progression toward its final value. The stable adjustment of K_d contributes to improved damping characteristics and reduced oscillatory behavior in the closed-loop system response.

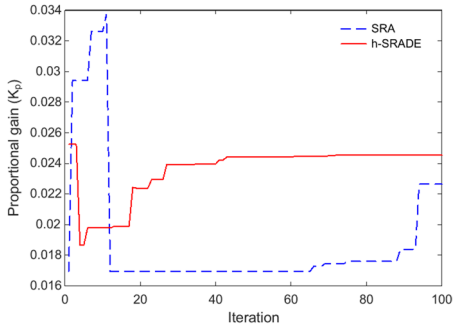


Fig. 7. Change of K_p parameter

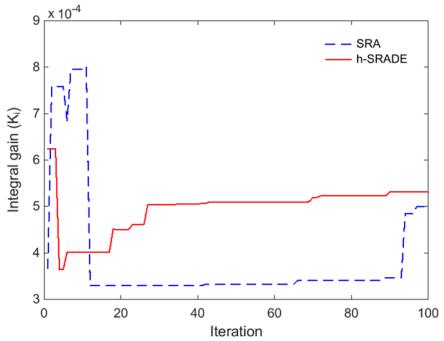


Fig. 8. Change of K_i parameter

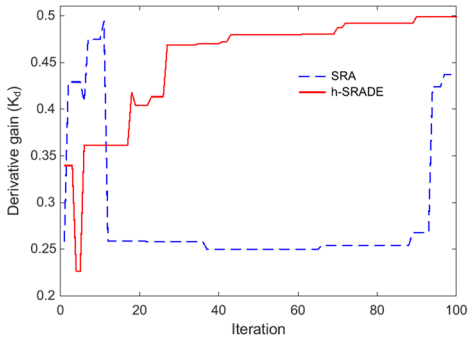


Fig. 9. Change of K_d parameter

Algorithm	K_p	K_i	K_d	Closed-loop transfer function
SRA	0.022641	0.00049943	0.43714	$\frac{0.4371s^2+0.02264s+0.0004994}{64s^4+9.6s^3+0.9171s^2+0.03064s+0.0004994}$
h-SRADE	0.024528	0.00053136	0.49902	$\frac{0.499s^2+0.02453s+0.0005314}{64s^4+9.6s^3+0.979s^2+0.03253s+0.0005314}$

Table 2. The controller parameters and the respective closed-loop transfer functions obtained via SRA and h-SRADE.

The final optimized PID controller parameters obtained by both algorithms are summarized in Table 2, along with the corresponding closed-loop transfer functions. As reported, the h-SRADE yields higher values of K_p, K_i, and K_d compared to the SRA, resulting in a modified closed-loop transfer function with improved dynamic characteristics. The denominator coefficients of the closed-loop system indicate enhanced damping and faster response dynamics when the controller parameters are tuned using h-SRADE. Overall, the convergence profiles

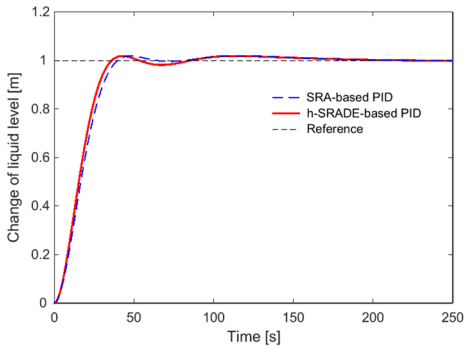


Fig. 10. Time response of SRA- and h-SRADE-based PID controlled systems for change of liquid level

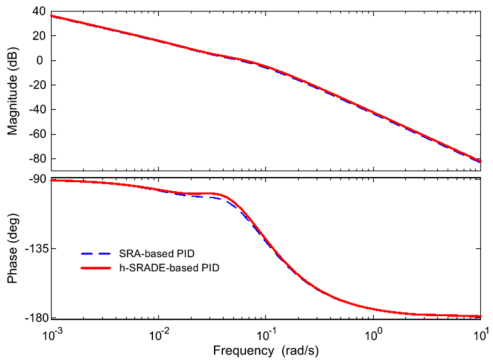


Fig. 11. Bode plot of SRA- and h-SRADE-based PID controlled systems

Algorithm	t_{set}(s)	m_{os}(%)	e_{ss}(%)	G_m(dB)	P_m(°)
SRA	36.9174	1.9724	0.0577	Inf	69.3674
h-SRADE	33.5102	1.8931	0.0437	Inf	68.1503

Table 3. Numerical results for time and frequency responses of SRA- and h-SRADE-based PID controllers.

and parameter evolution trends clearly demonstrate that the proposed h-SRADE not only achieves lower fitness values but also ensures smoother and more stable adaptation of PID controller parameters. These characteristics directly translate into improved closed-loop performance, providing a strong foundation for the time-domain and frequency-domain response analyses presented in the subsequent subsection.

Time and frequency responses

The time-domain and frequency-domain performances of the PID controllers optimized by SRA and the proposed h-SRADE are analyzed in this subsection. These analyses provide insight into the dynamic behavior and robustness of the closed-loop liquid level control system. The time response of the system to a unit step change in the reference liquid level is illustrated in Fig. 10. Both controllers successfully track the reference signal and ensure stable operation without sustained oscillations. However, the h-SRADE-based PID controller exhibits a noticeably faster transient response and reduced overshoot compared to the SRA-based counterpart. The system controlled by h-SRADE reaches the desired liquid level more rapidly and settles smoothly around the reference value, indicating improved damping characteristics.

The frequency-domain characteristics of the open-loop systems are shown in Fig. 11 using Bode magnitude and phase plots. Both controllers exhibit infinite gain margins ($G_m = \infty$), indicating strong robustness against gain variations. The phase margin of the SRA-based controller is 69.3674°, while the h-SRADE-based controller yields a phase margin of 68.1503°. Although a slight reduction in phase margin is observed, the obtained value remains sufficiently high to guarantee closed-loop stability and is accompanied by improved transient performance.

The numerical time-domain and frequency-domain performance indices obtained from these responses are summarized in Table 3, which reports the settling time (t_{set}), percent overshoot (m_{os}), percent steady-state error (e_{ss}), gain margin (G_m), and phase margin (P_m). As presented in the table, the h-SRADE-based controller achieves a reduced settling time of 33.5102 s, compared to 36.9174 s for the SRA-based controller. In addition,

Algorithm	K_p	K_i	K_d	Closed-loop transfer function
ALC-PSODE	0.0419	0.0009	1.0000	$\frac{s^2+0.0419s+0.0009}{64s^4+9.6s^3+1.48s^2+0.0499s+0.0009}$
AOA–HHO	0.0400	0.0005	0.4269	$\frac{0.4269s^2+0.04s+0.0005}{64s^4+9.6s^3+0.9069s^2+0.048s+0.0005}$
MGO	0.04168	0.00094	1.31334	$\frac{1.313s^2+0.04168s+0.00094}{64s^4+9.6s^3+1.793s^2+0.04968s+0.00094}$
MEASSA	0.1662	0.0198	3.9880	$\frac{3.988s^2+0.1662s+0.0198}{64s^4+9.6s^3+4.468s^2+0.1742s+0.0198}$

Table 4. Reported approaches in the literature and their relevant controller parameters and closed-loop transfer functions.

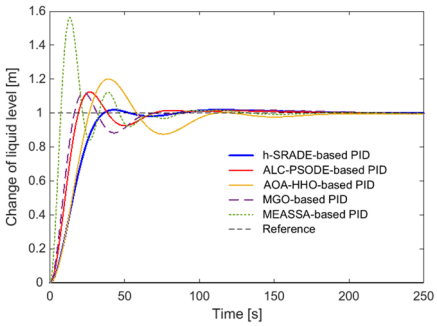


Fig. 12. Comparison with reported approaches in terms of step response for change of liquid level

the percent overshoot is decreased from 1.9724% to 1.8931%, and the steady-state error is reduced from 0.0577% to 0.0437%, confirming the superior tracking accuracy of the proposed approach. Overall, the results presented in Figs. 10 and 11, and Table 3 demonstrate that the h-SRADE-based PID controller offers enhanced time-domain performance while preserving adequate frequency-domain robustness. These improvements confirm the effectiveness of the proposed hybrid optimization strategy for liquid level control and provide a solid basis for the comparative analysis with existing approaches presented in the next subsection.

Comparison with reported works

In this subsection, the performance of the proposed h-SRADE-based PID controller is compared with several state-of-the-art approaches reported in the literature. The selected benchmark methods include hybrid differential evolution and particle swarm optimization with an aging leader and challengers (ALC-PSODE)[28], hybrid arithmetic and Harris hawks optimization (AOA–HHO)[29], mountain gazelle optimization (MGO)[23] and enhanced artificial satellite search algorithm with memory and evolutionary operator (MEASSA)[30]. These approaches have been widely adopted for PID controller tuning in liquid level and related control systems and therefore provide a meaningful basis for comparison.

The PID controller parameters and the corresponding closed-loop transfer functions reported for these methods are summarized in Table 4. It can be observed that the reported approaches employ significantly different gain combinations, leading to distinct closed-loop dynamics. In particular, methods such as MEASSA and MGO rely on relatively large derivative gains, which tend to amplify oscillatory behavior and adversely affect transient performance.

The time-domain responses of the closed-loop liquid level system for all compared methods are illustrated in Fig. 12. As shown, the h-SRADE-based PID controller achieves a faster rise and settling behavior with noticeably reduced overshoot when compared to the reported approaches. Methods such as AOA–HHO and MEASSA exhibit pronounced oscillations and longer settling periods, whereas ALC-PSODE and MGO show slower convergence toward the reference level.

To further highlight steady-state performance, a magnified view of the system response near the final simulation interval is presented in Fig. 13. The h-SRADE-based controller maintains the closest tracking to the reference level with the smallest steady-state deviation. In contrast, the other approaches exhibit larger steady-state errors, particularly AOA–HHO and MEASSA, indicating inferior regulation accuracy.

The frequency-domain characteristics of the compared controllers are depicted in Fig. 14 using Bode magnitude and phase plots. The h-SRADE-based controller demonstrates favorable robustness properties, with smooth magnitude attenuation and a sufficiently large phase margin. Although most reported methods exhibit infinite gain margins, the phase margins of ALC-PSODE, AOA–HHO, MGO, and MEASSA are considerably lower than that of h-SRADE, which indicates reduced tolerance to phase uncertainties and disturbances.

The quantitative comparison of time-domain and frequency-domain performance indices is summarized in Table 5. The h-SRADE-based PID controller achieves the shortest settling time (33.5102 s), the lowest percent

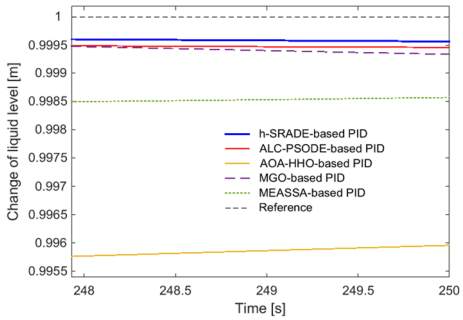


Fig. 13. Comparison with reported approaches in terms of steady-state error for change of liquid level

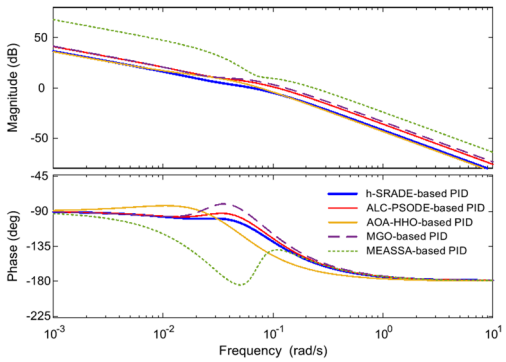


Fig. 14. Comparison with reported approaches in terms of Bode plot

Algorithm	t_{set}(s)	m_{os}(%)	e_{ss}(%)	G_m(dB)	P_m(°)
h-SRADE	33.5102	1.8931	0.0437	Inf	68.1503
ALC-PSODE	64.2147	12.4682	0.0543	Inf	51.6652
AOA–HHO	160.1083	20.1179	0.4044	Inf	43.1866
MGO	60.5703	12.1153	0.0665	Inf	49.4766
MEASSA	82.1266	56.2397	0.1427	− 16.2076	25.2840

Table 5. Comparative numerical results for time and frequency responses with respect to reported works.

overshoot (1.8931%), and the smallest steady-state error (0.0437%) among all compared methods. Moreover, it preserves an infinite gain margin and a relatively high phase margin (68.1503°), ensuring robust closed-loop stability. In contrast, the reported methods suffer from significantly longer settling times, larger overshoot values, and, in the case of MEASSA, a negative gain margin, which indicates poor robustness. Overall, the comparative results presented in Tables 4, 5 and Figs. 12, 13, 14 clearly demonstrate that the proposed h-SRADE-based PID controller outperforms the reported state-of-the-art approaches in terms of transient response speed, steady-state accuracy, and robustness. These findings confirm the effectiveness of the proposed hybrid optimization strategy for liquid level control systems and highlight its superiority over existing methods reported in the literature.

Quality indicator comparison

In this subsection, a comparative evaluation of the quality indicator is presented using the fitness function defined in Eq. (21). The fitness function serves as a unified performance index that simultaneously reflects transient response characteristics and steady-state accuracy. Since lower fitness values correspond to superior overall control performance, the comparison provides a concise and meaningful assessment of different optimization approaches. The comparative fitness function values obtained for the proposed h-SRADE and the reported approaches are illustrated in Fig. 15. As observed, the h-SRADE-based PID controller achieves the lowest fitness value ($FF = 4.1068$) among all considered methods, indicating the most balanced trade-off between overshoot, steady-state error, settling time, and rise time. The conventional SRA follows with a slightly higher fitness value ($FF = 4.5501$), confirming the improvement introduced by the hybridization with differential evolution operators. In contrast, the reported methods exhibit significantly larger fitness values. The ALC-PSODE approach yields an FF of 19.0076, while MGO results in an FF of 18.3231, reflecting slower dynamic

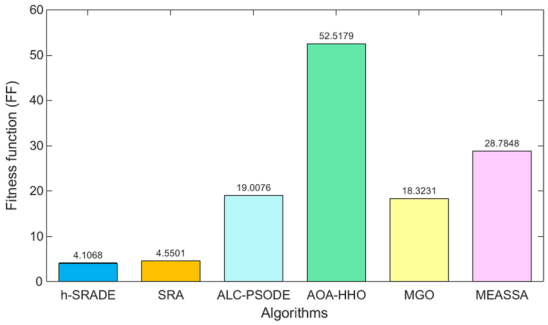


Fig. 15. Comparative fitness function evaluation with respect to reported works

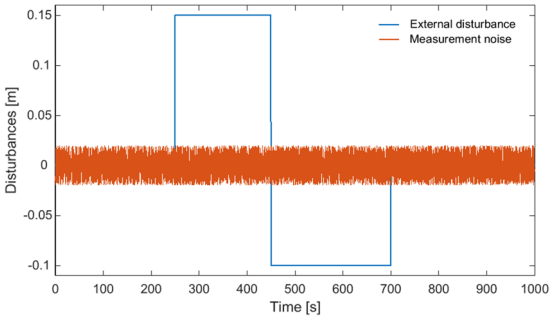


Fig. 16. External disturbance and measurement noise signals applied in the disturbance rejection simulation

responses and inferior steady-state accuracy. The AOA–HHO and MEASSA methods show substantially higher fitness values of 52.5179 and 28.7848, respectively, which are mainly attributed to excessive overshoot, prolonged settling times, and degraded steady-state performance observed in the corresponding time-domain responses. Overall, the results presented in Fig. 15 clearly demonstrate the superiority of the proposed h-SRADE-based PID controller in terms of the adopted quality indicator. The marked reduction in the fitness function confirms that the proposed hybrid optimization framework delivers a more effective balance between dynamic response speed and regulation accuracy compared with both the original SRA and the state-of-the-art methods reported in the literature. This outcome further validates the effectiveness and robustness of the proposed approach for liquid level control applications.

Disturbance rejection analysis

To provide a more comprehensive assessment of the h-SRADE-based PID controller, an explicit disturbance rejection simulation is conducted in this subsection. The capability to recover from external perturbations and measurement noise is of particular importance in liquid level control applications, where load variations and sensor noise are routinely encountered and may prove operationally more consequential than setpoint tracking alone. In the present simulation, two disturbance signals are applied simultaneously to the closed-loop system over a total simulation horizon of 1000 s, following an initial period of setpoint tracking. The external disturbance is modeled as a square wave signal with an amplitude of ± 0.15 m, representative of sudden changes in outflow conditions (such as step variations in q_1 or q_2), and is applied at $t = 250s$ and $t = 450s$, with polarity reversals at $t = 450s$ and $t = 700s$, respectively. In addition, band-limited measurement noise with a power spectral density of 0.001 m^2/Hz is superimposed on the output signal throughout the entire simulation to emulate realistic sensor uncertainty. The applied disturbance and noise signals are illustrated in Fig. 16.

The resulting closed-loop liquid level response under these combined perturbations is presented in Fig. 17. Upon the onset of the positive external disturbance at t = 250 s, the liquid level deviates transiently from the reference, reaching a peak overshoot of approximately 1.14 m before the controller initiates recovery. The h-SRADE-based PID controller effectively suppresses this perturbation and restores the liquid level to the vicinity of the 1 m reference within a short recovery interval. When the disturbance polarity reverses at t = 450 s, a transient undershoot to approximately 0.77 m is observed, after which the controller again drives the output back toward the reference. A further recovery event occurs at t = 700 s, following the cessation of the square wave disturbance, with the liquid level returning promptly to the setpoint. Throughout the entire simulation, the influence of measurement noise is continuously attenuated by the closed-loop action of the controller, with only minor fluctuations visible in the steady-state output. These results confirm that the h-SRADE-optimized PID controller possesses satisfactory disturbance rejection capability in addition to the setpoint tracking performance demonstrated in the preceding subsections. The integral action of the PID structure ensures zero steady-state offset following each disturbance event, while the optimized derivative and proportional gains contribute to

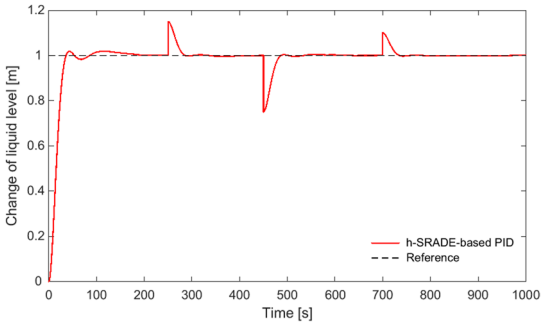


Fig. 17. Closed-loop liquid level response of the h-SRADE-based PID controller under simultaneous external disturbance and measurement noise

adequate damping of the transient deviations. It is also observed that the measurement noise does not induce controller chattering or instability, which is attributable in part to the moderate derivative gain obtained through the h-SRADE optimization process. Collectively, the disturbance rejection analysis presented here provides additional evidence of the practical robustness of the proposed control framework, complementing the frequency-domain robustness margins reported in Section "Time and frequency responses" and reinforcing the overall effectiveness of the h-SRADE-based PID controller for liquid level regulation under realistic operating conditions.

Conclusion

In this study, a hybrid Schrödinger optimizer with differential evolution, abbreviated as h-SRADE, has been proposed and applied to the optimal tuning of a PID controller for a three-tanks liquid level control system. The original Schrödinger optimizer, inspired by wave–particle duality, offers an effective balance between exploration and exploitation; however, its sensitivity in the final convergence phase motivated further enhancement. To overcome this limitation, differential evolution mutation and crossover operators were integrated into the Schrödinger optimization framework, resulting in the proposed h-SRADE algorithm with improved refinement capability and convergence robustness. The liquid level control problem was formulated using a linearized third-order model derived from mass balance principles. PID controller parameters were optimized through a composite fitness function that simultaneously accounts for transient and steady-state performance indices, including percent overshoot, steady-state error, settling time, and rise time. Practical parameter bounds were enforced to ensure controller feasibility and reliable closed-loop operation. Extensive simulation studies demonstrated the effectiveness of the proposed approach. Statistical analysis based on multiple independent runs, supported by a non-parametric Wilcoxon signed-rank test, confirmed the statistical significance and robustness of h-SRADE in comparison with the conventional Schrödinger optimizer. Convergence behavior and parameter evolution analyses showed that the hybrid method achieves smoother and more stable adaptation of PID gains. Time-domain results indicated faster settling, reduced overshoot, and lower steady-state error, while frequency-domain analysis confirmed that adequate robustness margins were preserved. Furthermore, comparative evaluations against several state-of-the-art optimization-based PID tuning approaches reported in the literature revealed that the h-SRADE-based controller consistently outperforms existing methods in terms of dynamic response speed, regulation accuracy, and overall control quality. The proposed method also achieved the lowest value of the adopted fitness function, demonstrating a superior balance between competing performance objectives. Overall, the results confirm that hybridizing the Schrödinger optimizer with differential evolution significantly enhances optimization efficiency and control performance. It should be acknowledged, however, that the findings reported in this study were obtained through simulation studies conducted on a linearized third-order representation of the three-tank liquid level system, so that the demonstrated improvements in convergence behavior and closed-loop performance are established within the scope of this linearized framework. Although the linearization was performed about a representative operating point and follows established practice for controller design and benchmarking in this class of systems, the transition to the underlying nonlinear plant or to a physical experimental setup may introduce additional effects, including actuator saturation, unmodeled nonlinear dynamics, and sensor or measurement uncertainties, which were not captured in the present analysis and which could influence the closed-loop behavior of the h-SRADE-tuned controller. Within this scope, the proposed h-SRADE framework provides a reliable and effective solution for PID controller tuning in liquid level systems, and the performance gains demonstrated here constitute a sound basis for further validation under nonlinear and experimental conditions.

Future work may focus on extending the proposed approach to nonlinear or time-varying models, experimental validation on real-time platforms, and application to other complex engineering control problems. From a longer-term perspective, the emerging body of rigorously grounded quantum optimization algorithms[42–44] offers a theoretically principled foundation from which future quantum-inspired metaheuristics may draw more structured design principles, particularly as the boundary between pure quantum algorithms and classical-hardware optimizers continues to be explored.

Data availability

All related data are presented within the manuscript.

Received: 4 January 2026; Accepted: 24 August 2026
Published online: 02 September 2026

References

1. Jiang, K. Enhancing water level system based on fuzzy PID control. *J. Phys. Conf. Ser.* **2786**, 012014 (2024).
2. Luyben, W. L. Liquid level control: Simplicity and complexity. *J. Process Control* **86**, 57–64 (2020).
3. Başçi, A. & Derdiyok, A. Implementation of an adaptive fuzzy compensator for coupled tank liquid level control system. *Measurement* **91**, 12–18 (2016).
4. Pan, H., Wong, H., Kapila, V. & de Queiroz, M. S. Experimental validation of a nonlinear backstepping liquid level controller for a state coupled two tank system. *Control Eng. Pract.* **13**, 27–40 (2005).
5. Cheung, T.-F. Liquid-level control in single tanks and cascades of tanks with proportional-only and proportional-integral feedback controllers. *Ind. Eng. Chem. Fundam.* **18**, 15–21 (1979).
6. Dlabač, T., Antić, S., Ćalasan, M., Milovanović, A. & Marvučić, N. Nonlinear tank-level control using Dahlin algorithm design and PID control. *Appl. Sci.* **13**, 5414 (2023).
7. Cartes, D. & Wu, L. Experimental evaluation of adaptive three-tank level control. *ISA Trans.* **44**, 283–293 (2005).
8. Srinivasan, K., Devassy, J. & Dhanapal, S. Level control of three-tank system using intelligent techniques. *Int. J. Image Min.* **2**, 318 (2017).
9. Yu, S. et al. Liquid level tracking control of three-tank systems. *Int. J. Control Autom. Syst.* **18**, 2630–2640 (2020).
10. Yu, H., Yu, J., Wu, H. & Li, H. Energy-shaping and integral control of the three-tank liquid level system. *Nonlinear Dyn.* **73**, 2149–2156 (2013).
11. Dormido, R. et al. Development of a web-based control laboratory for automation technicians: The three-tank system. *IEEE Trans. Educ.* **51**, 35–44 (2008).
12. Singh, S., Singh, V. P., Dohare, R. K., Singh, S. P. & Jain, S. K. Optimal PID controller design for level control of three tank system. *Int. J. Adv. Technol. Eng. Explor.* **4**, 1–5 (2016).
13. Idir, A., Nesri, M., Belhouchet, K., Guedida, S. & Canale, L. Enhancing the transient performances and stability of three-tank liquid level using a modified PID controller. *Revue Roumaine des Sciences Techniques — Série Électrotechnique et Énergétique* **70**, 567–572 (2025).
14. Sharma, A., Goud, H. & Kar, M. K. 3-tank system liquid level control using metaheuristic algorithm. in *2023 IEEE Renewable Energy and Sustainable E-Mobility Conference (RESEM)* 1–5 (IEEE, 2023). https://doi.org/10.1109/RESEM57584.2023.10236010.
15. Izci, D. & Ekinci, S. Optimizing three-tank liquid level control: Insights from prairie dog optimization. *Int. J. Robot. Control Syst.* **3**, 599–608 (2023).
16. Rojas, J. D., Arrieta, O. & Vilanova, R. *Industrial PID Controller Tuning* (Springer International Publishing, 2021). https://doi.org/10.1007/978-3-030-72311-8.
17. Nisi, K., Nagaraj, B. & Agalya, A. Tuning of a PID controller using evolutionary multi objective optimization methodologies and application to the pulp and paper industry. *Int. J. Mach. Learn. Cybern.* **10**, 2015–2025 (2019).
18. Blevins, T. L. PID advances in industrial control. *IFAC Proc. Vol.* **45**, 23–28 (2012).
19. Bennett, S. Development of the PID controller. *IEEE Control Syst.* **13**, 58–62 (1993).
20. Wu, Y., Xing, L., Guo, F. & Liu, X. On the combination of PID control and reinforcement learning: A case study with water tank system. in *2021 IEEE 16th Conference on Industrial Electronics and Applications (ICIEA)* 1877–1882 (IEEE, 2021). https://doi.org/10.1109/ICIEA51954.2021.9516140.
21. Chen, X. *et al.* 3-Tank system liquid level control using improved african vulture optimization algorithm. in *2024 7th International Conference on Energy, Electrical and Power Engineering (CEEPE)* 635–641 (IEEE, 2024). https://doi.org/10.1109/CEEPE62022.2024.10586359.
22. Long, F., Yao, Y., Zhou, Y. & He, J. Simulation analysis of three-tank water tank level control system based on improved PSO-fuzzy PID. in *2024 5th International Seminar on Artificial Intelligence, Networking and Information Technology (AINIT)* 1833–1837 (IEEE, 2024). https://doi.org/10.1109/AINIT61980.2024.10581741.
23. Ekinci, S. et al. Advanced control parameter optimization in DC motors and liquid level systems. *Sci. Rep.* **15**, 1394 (2025).
24. Jatoth, R. K., Jain, A. K. & Phanindra, T. Liquid level control of three tank system using hybrid GA-PSO algorithm. in *2013 Nirma University International Conference on Engineering (NUiCONE)* 1–7 (IEEE, 2013). https://doi.org/10.1109/NUiCONE.2013.6780189.
25. Chelouah, R. & Siarry, P. Genetic and Nelder-Mead algorithms hybridized for a more accurate global optimization of continuous multiminima functions. *Eur. J. Oper. Res.* **148**, 335–348 (2003).
26. Nenavath, H. & Jatoth, R. K. Hybridizing sine cosine algorithm with differential evolution for global optimization and object tracking. *Appl. Soft Comput.* **62**, 1019–1043 (2018).
27. Zubaidi, S. L. et al. Hybridised artificial neural network model with slime mould algorithm: A novel methodology for prediction of urban stochastic water demand. *Water* **12**, 2692 (2020).
28. Moharam, A., El-Hosseini, M. A. & Ali, H. A. Design of optimal PID controller using hybrid differential evolution and particle swarm optimization with an aging leader and challengers. *Appl. Soft Comput.* **38**, 727–737 (2016).
29. Issa, M. Enhanced arithmetic optimization algorithm for parameter estimation of PID controller. *Arab. J. Sci. Eng.* **48**, 2191–2205 (2023).
30. Issa, M. Enhanced artificial satellite search algorithm with memory and evolutionary operator for PID controller parameter estimation. *Sci. Rep.* **15**, 39551 (2025).
31. Hussein, N. K. et al. Schrödinger optimizer: A quantum duality-driven metaheuristic for stochastic optimization and engineering challenges. *Knowl. Based. Syst.* **328**, 114273 (2025).
32. Price, K. V., Storn, R. M. & Lampinen, J. A. *Differential Evolution*. *Differential Evolution* (Springer-Verlag, Berlin/Heidelberg, 2005). https://doi.org/10.1007/3-540-31306-0.
33. Wei, Y. A Hybrid evolutionary algorithm based on Artificial Bee Colony algorithm and Differential Evolution. in *2021 2nd International Conference on Computer Engineering and Intelligent Control (ICCEIC)* 35–40 (IEEE, 2021). https://doi.org/10.1109/ICCEIC54227.2021.00015.
34. Ali, M., Pant, M. & Abraham, A. A simplex differential evolution algorithm: Development and applications. *Trans. Inst. Meas. Control* **34**, 691–704 (2011).
35. Luitel, B. & Venayagamoorthy, G. K. Differential evolution particle swarm optimization for digital filter design. in *2008 IEEE Congress on Evolutionary Computation (IEEE World Congress on Computational Intelligence)* 3954–3961 (IEEE, 2008). https://doi.org/10.1109/CEC.2008.4631335.
36. Das, S. & Suganthan, P. N. Differential evolution: A survey of the state-of-the-art. *IEEE Trans. Evol. Comput.* **15**, 4–31 (2011).
37. Biswas, S. et al. A novel hybrid optimizer based on coati optimization algorithm and differential evolution for global optimization and constrained engineering problems. *Int. J. Comput. Intell. Syst.* **18**, 157 (2025).

38. Ekinci, S., Izci, D., Kayri, M., Elsayed, F. & Salman, M. A novel hybridization of birds of prey-based optimization with differential evolution mutation and crossover for chaotic dynamics identification. *Sci. Rep.* **15**, 43451 (2025).
39. Maiti, B. et al. Enhanced crayfish optimization algorithm with differential evolution's mutation and crossover strategies for global optimization and engineering applications. *Artif. Intell. Rev.* **58**, 69 (2025).
40. Güven, A. F., Mengi, O. Ö., Elseify, M. A. & Kamel, S. Comprehensive optimization of PID controller parameters for DC motor speed management using a modified jellyfish search algorithm. *Optimal Control Appl. Methods* **46**, 320–342 (2025).
41. Izci, D. et al. Enhanced hiking optimization algorithm for robust PID control in doubly-fed induction generator systems for wind energy applications. *IET Control Theory Appl.* **19**, e70071 (2025).
42. Chen, Z., Lu, Y., Wang, H., Liu, Y. & Li, T. Quantum Langevin dynamics for optimization. *Commun. Math. Phys.* **406**, 52 (2025).
43. Leng, J., Hickman, E., Li, J. & Wu, X. Quantum hamiltonian descent. arXiv preprint arXiv:2303.01471 (2023).
44. Leng, J. & Shi, B. Quantum optimization via gradient-based Hamiltonian descent. in *Gavriel Salvendy International Symposium on Frontiers in Industrial Engineering Purdue Quantum AI* 170–177 (Springer, 2025).

Author contributions

Davut Izci, Serdar Ekinci: Conceptualization, Methodology, Software, Visualization, Investigation, Writing – Original Draft. İrfan Ökten, Vedat Tümen, Mostafa Rashdan, Mohammad Salman: Data Curation, Validation, Supervision, Resources, Writing – Review & Editing.

Funding

This research received no specific grant from any funding agency in the public, commercial, or not-for-profit sectors.

Declarations

Competing interests

The authors declare no competing interests.

Additional information

Correspondence and requests for materials should be addressed to M.S.

Reprints and permissions information is available at www.nature.com/reprints.

Publisher's note Springer Nature remains neutral with regard to jurisdictional claims in published maps and institutional affiliations.

Open Access This article is licensed under a Creative Commons Attribution-NonCommercial-NoDerivatives 4.0 International License, which permits any non-commercial use, sharing, distribution and reproduction in any medium or format, as long as you give appropriate credit to the original author(s) and the source, provide a link to the Creative Commons licence, and indicate if you modified the licensed material. You do not have permission under this licence to share adapted material derived from this article or parts of it. The images or other third party material in this article are included in the article's Creative Commons licence, unless indicated otherwise in a credit line to the material. If material is not included in the article's Creative Commons licence and your intended use is not permitted by statutory regulation or exceeds the permitted use, you will need to obtain permission directly from the copyright holder. To view a copy of this licence, visit http://creativecommons.org/licenses/by-nc-nd/4.0/.

© The Author(s) 2026